J Sol-Gel Sci Techn (2006) 40:3–8
DOI 10.1007/s10971-006-9114-z

Comparative study of the textural and structural properties of the aerogel and xerogel sulphated zirconia

Imene Mejri · Mohamed Kadri Younes · Abdelhamid Ghorbel

Received: 8 September 2005 / Accepted: 12 May 2006 / Published online: 22 August 2006

Abstract Aerogel and xerogel sulphated zirconia with defined atomic ratio S/Zr = 0.5 and molar hydrolysis ratio $h = nH_2O/nZrO_2 = 3$ show different textural and structural properties after calcination at high temperatures. The aerogel obtained just after solvent evacuation develops only the tetragonal phase, whereas the xerogel dried in an oven is amorphous. Heating to a temperature above 833 K, leads to transition of the tetragonal phase to the monoclinic one for the two solids, due to sulphur loss but the tetragonal phase remains stable for the aerogel . Raman, Infrared and XPS spectroscopies show that the loss of the sulphur at high temperatures seems to be easier for the xerogel than for the aerogel.

Keywords Sulphated zirconia · Aerogel · Xerogel · Sulphate species

1. Introduction

Since its discovery by Hino and Arata, sulphated zirconia has drawn the attention of many researchers as it exhibits an important acidity [1]. This acid strength which is equal to that of sulphuric acid [2–4] confers to sulphated zirconia excellent catalytic properties in many reactions [5, 6], including isomerization [7–9], cracking [10], alkylation [11, 12] and Friedel-crafts acylation [13, 14]. Many papers have dealt with the elaboration of sulphated zirconia [15–17]. The common one is the impregnation of ZrO_2 by H_2SO_4 or $(NH_4)_2SO_4$ solutions [18–21], but the resulting solids exhibit a low surface area.

Sulphated zirconia has also been prepared by one step synthesis using the sol gel method [22, 23]; in this case the preparation process is well controlled by the hydrolysis and condensation steps. The resulting materials exhibit a large surface area and high porosity. Evacuation of the solvent within the wet gel can be done either by simple drying in an oven, leading to the xerogel, or under the hypercritical conditions of the solvent, leading to the aerogel.

In our previous work [24–26] we showed that the hydration and sulphating steps were very important in the control of the texture and structure of the aerogels. The main purpose of this work is to study the impact of two solvent evacuation ways on the structural and textural properties of sulphated zirconia.

2. Experimental

2.1. Catalysts preparation

ZrO_2-SO_4^{2-} (ZS) solids were prepared as follows: First, Zirconium (IV) propoxide (70% in propanol, Aldrich) dissolved in 1-propanol was sulphated with concentrated H_2SO_4 in such an amount as to give the molar ratio S/Zr = 0.5 and stirred for one hour. Water was then slowly added drop-wise to obtain a gel with hydrolysis molar ratio $h = H_2O/Zr = 3$. The gel was then divided into two parts. The xerogel was obtained by overnight drying at 393 K in an oven, whereas the aerogel was obtained under the supercritical conditions of 1-propanol in an autoclave ($P = 51$ bar $T = 536{,}6$ K). The resulting solids were then calcined under a flow of oxygen

I. Mejri (✉) · M. K. Younes · A. Ghorbel
Laboratoire de Chimie des Matériaux et Catalyse, Département de Chimie, Faculté des Sciences de Tunis Campus universitaire, 2092 ElManar, Tunis, Tunisia
e-mail: mejriimene@yahoo.fr

at different temperatures in the temperature range of 573–973 K.

2.2. Characterization

XRD patterns were obtained on a Siemens D-5000 powder diffractometer using Ni-filtered Cu Kα radiation ($\lambda =$ 1,5418 Å). The scan rate was 0. 02° per second for 2θ from 5° to 70°.

Adsorption-desorption isotherms of N_2 at 77 K were performed with a Micromeritics ASAP 2000 apparatus after outgassing the solids at 473 K for three hours. The specific surface area and pore size distribution were determined by BET and BJH methods. The errors in the surface area measurments are 5%.

The FTIR spectra of the samples calcined at different temperatures and diluted in KBr were recorded with a Perkin Elmer Pragon 1000PC spectrometer.

The XPS results were obtained with a SSI X probe spectrometer (model SSX 100, Surface Science Laboratories, Mountain View, CA). The source was monochromatic AlK_α radiation (1486 eV).

Raman spectra were performed with the Perkin Elmer System 2000 NIR FT-Raman. The excitation radiation was 5th harmonic of a diode pumped Nd: YAG laser (1065 nm).

3. Results and discussion

N_2 isotherms and pore size distribution of the aerogel and xerogel are given in Figs. 1 and 2.

N_2 isotherm of the aerogel shows a type IV behaviour, characteristic of mesoporous materials, with a H3 hysteresis loop [27] corresponding to particles having a sheet structure. The pore size distribution is wide, monomodal and centred around 25 nm.

N_2 isotherm of the xerogel shows a type IV behaviour, characteristic of mesoporous materials, with a H4 hysteresis loop [27] corresponding to particles having a sheet structure. The pore size distribution is bimodal with pores having diameter between 3–5 nm.

The BET surface area and average pore diameter of the aerogel and xerogel are compiled in Table 1.

The average pore diameter of the aerogel is higher than that of the xerogel. This difference can be explained by the solvent evacuation mode. In fact, the solvent evacuation by simple evaporation in an oven is susceptible to form a liquid-vapour interface within the gel. This creates a surface tension which acts on the pores and causes them to shrink. However, when the solvent is removed under its hypercritical conditions, the liquid-vapour interface is avoided and the absence of the surface tension allows the gel to be dried without shrinkage of the pores. The average pore

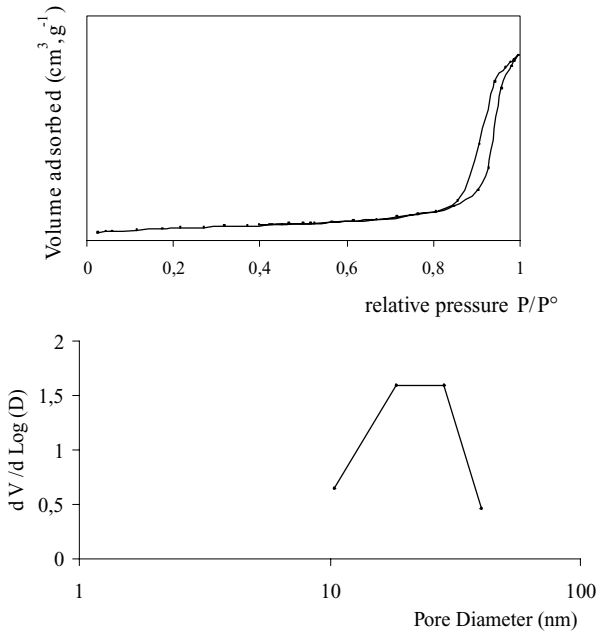

Fig. 1 Adsorption-desorpotion isotherm and BJH pore distribution of the aerogel

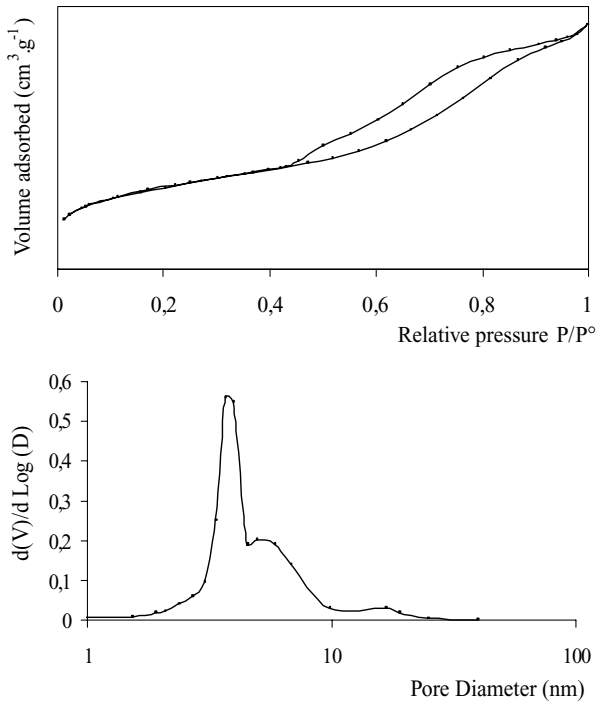

Fig. 2 Adsorption-desorpotion isotherm and BJH pore distribution of the xerogel

diameter remains almost constant in the investigated calcination temperature range either for the aerogel or for the xerogel.

The surface area of the aerogel remains almost constant in the temperature range of 833–923 K and decreases at 973 K, whereas the surface area of the xerogel remains constant at 833 and 873 K. Then a drastic decrease is noted at 923 K. It

Table 1 Textural properties of the aerogel and xerogel calcined at different temperatures

	Aerogel		Xerogel	
T (K)	S_{BET} (m^2/g)	D_p (nm)	S_{BET} (m^2/g)	D_p (nm)
573	122	23,7	–	–
833	109	26,0	100	4,1
873	111	25,6	92	4,3
923	103	22,7	54	4,5
973	74	22,5	48	4,7

D_p: Average pore diameter.

has been reported that the decrease in the surface area is due to the loss of sulphur during the calcination step [28]. This is expressed by the transition of the tetragonal phase to the monoclinic one. It has also been reported that the presence of sulphur preserves the surface area after calcination [29–32]. We can assume that the decrease in the surface area of the xerogel at 923 K before the aerogel is due to the loss of sulphate during the calcination step.

Figures 3 and 4 show the X-ray diffraction patterns of the aerogel and xerogel, calcined at different temperatures.

The aerogel obtained just after solvent evacuation without further heating is well crystallized and exhibits the tetragonal phase, characterized by the diffraction peaks at $2\theta = 30°, 50°$ and $60°$ whereas, the xerogel dried at 393 K is amorphous. The same situation is observed after calcination at 573 K.

Heating at higher temperatures, leads to the monoclinic phase characterized by the diffraction peaks at $2\theta = 24°, 28°$ and $31°$ in the two solids but, this phase is more developed for the xerogel. In fact, X-Ray diffraction of the aerogel reveals the tetragonal phase at the calcination temperature range 573–873 K, and the relative ratio of the monoclinic phase is very low at 923 K and increases slowly at higher temperatures. On the other hand X-Ray diffraction of the xerogel reveals the tetragonal phase and the monoclinic phase, which appears at 873 K and increases at higher temperatures.

The aerogel develops the tetragonal phase under high pressure during the evacuation step. Calcination at higher temperatures preserves this phase and only a small amount of the monoclinic phase was observed. Transition of the tetragonal phase to the monoclinic one is related to the loss of sulphur, and therefore the tetragonal phase is thought to be stabilized by sulphate species [33–35]. Thus, we can assume

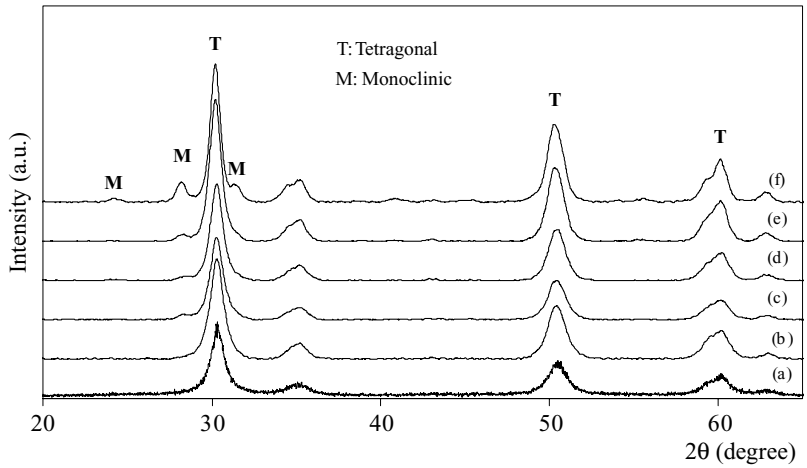

Fig. 3 XRD patterns of the aerogel calcined at different temperatures: (a) non calcined; (b) 573 K, (c) 833 K, (d) 873 K, (e) 923 K, (f) 973 K

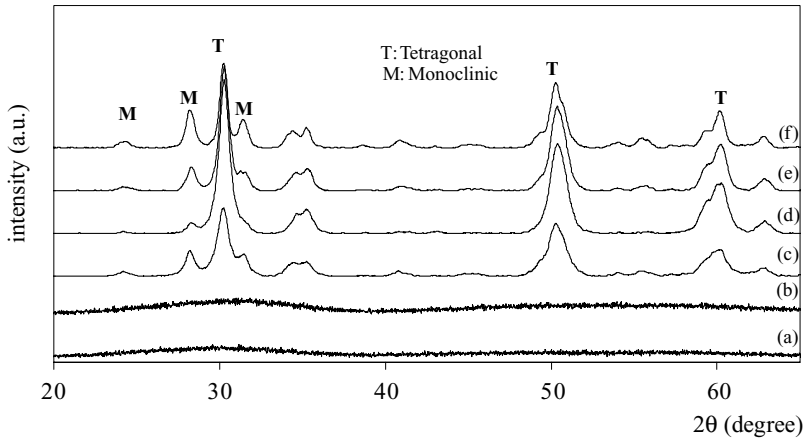

Fig. 4 XRD patterns of the xerogel calcined at different temperatures: (a) non calcined; (b) 573 K, (c) 833 K, (d) 873 K, (e) 923 K, (f) 973 K

Table 2 Attribution of the IR bands of the aerogel and xerogel

Aerogel		Xerogel	
Bands (cm^{-1})	Attribution	Bands (cm^{-1})	Attribution
3420	OH vibration [39, 40]	3424	OH vibration [39, 40]
1629	δ_{HOH} [40]	1631	δ_{HOH} [40]
563, 491, 415	Crystalline zirconia [40]	592, 494, 427	Crystalline zirconia [40]
1071	$(\delta_{S-O})_{as}$ of S–O [41, 42]	1131	$(\delta_{S-O})_{as}$ S–O [41, 42]
1381	ν S=O or asymmetric stretching mode of O=S=O [43]	1385	ν S=O or asymmetric stretching mode of O=S=O [43]
1200	Symmetric stretching mode of O=S=O [43]	1266	Symmetric stretching mode of O=S=O [43]
1208, 1128, 1040, 1002	ν_1 and ν_3 vibration modes of sulphate species [43, 44]	1110	ν_1 and ν_3 vibration modes of sulphate species [43, 44]

that the sulphate species in the aerogel are retained more strongly than those in the xerogel.

The aerogel and the xerogel exhibit different results: the tetragonal zirconia is predominant in the aerogel whereas the monoclinic phase is more developed in the xerogel. This result allows us to consider that the loss of sulphur induces the transformation of the tetragonal into the monoclinic phase and that the modifications in the textural properties and the appearance of the monoclinic phase are two related phenomena.

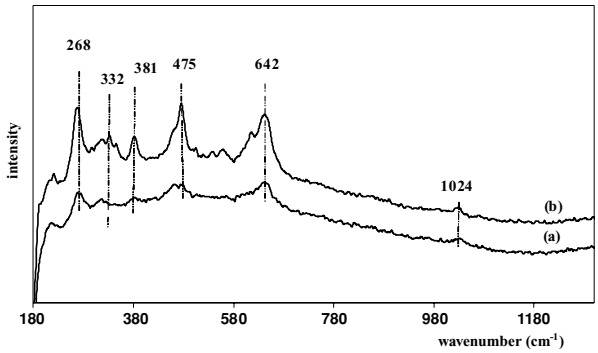

Fig. 5 Raman spectra of the aerogel calcined at: (a) 833, (b) 923

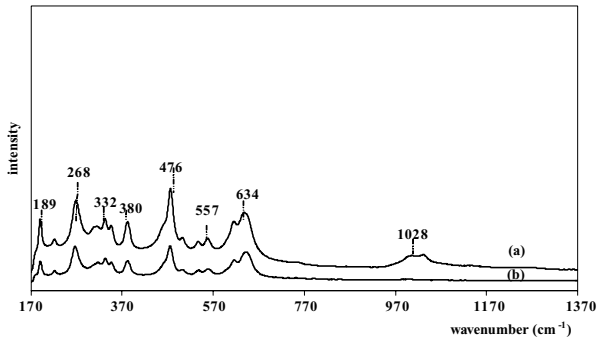

Fig. 6 Raman spectra of xerogel calcined at: (a) 833, (b) 923

Raman spectra of the aerogel and xerogel calcined at 833 K and 923 K are illustrated in Figs. 5 and 6.

According to the literature [36–38], the bands which are characteristic of the monoclinic zirconia are at 189, 332, 557 cm^{-1}, by contrast, the band at 268 cm^{-1} is assigned to the tetragonal zirconia. The doublet 476–634 cm^{-1} is attributed to the monoclinic zirconia when the band at 476 cm^{-1} is more intense, and to the tetragonal phase when the two bands show the same intensity. The bands at 1028 cm^{-1} and 1130 cm^{-1} correspond to the symmetric and asymmetric vibrations of sulphated groups [36]. Our experiments (Figs. 5 and 6) show the presence of both phases.

Upon calcination at 923 K, the bands of sulphate disappear in the xerogel showing the decomposition of the sulphate groups. This phenomenon is much less marked in the aerogel.

The FTIR spectra of the aerogel and xerogel calcined at 833 K and 923 K are given in Figs. 7 and 8.

Attribution of the bands of the aerogel and xerogel are reported in Table 2.

The xerogel calcined at 833 K has the same bands observed in the aerogel, but less intense and the band attributed to S–O $(\delta_{S-O)as}$ is large and shifted to 1131 cm^{-1}. Calcination at 923 K causes the decrease in the band intensities, and the bands characterizing ν_1 and ν_3 vibration modes of sulphate species appear at 1208 cm^{-1}, 1128 cm^{-1}, 1040 cm^{-1} and 1002 cm^{-1} [43, 44] in the aerogel, whereas, many bands characterizing the sulphate groups disappear in the xerogel. This result suggests that the sulphate species are more stable at higher temperature for the aerogel.

Table 3 Surface S/Zr ratio of the aerogel and xerogel

T (K)	Aerogel	Xerogel
833	0.20	0.14
923	0.11	0.09

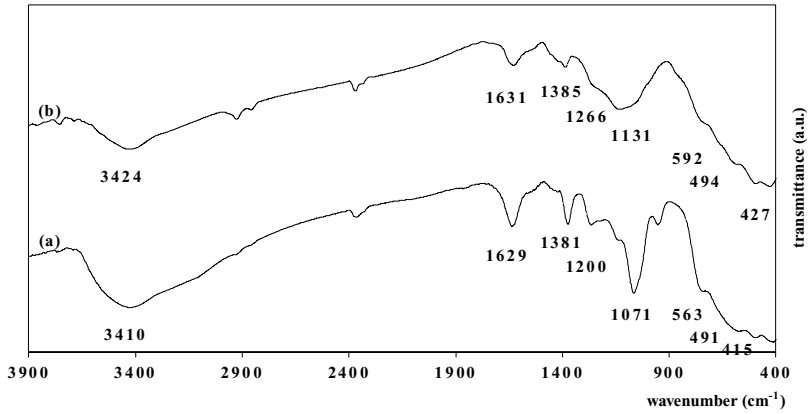

Fig. 7 IR spectra of the aerogel and the xerogel calcined at 833 K (a) aerogel, (b) xerogel

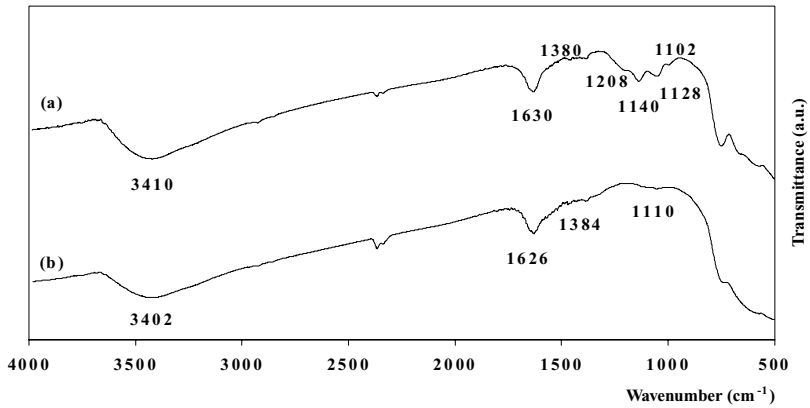

Fig. 8 IR spectra of the aerogel and the xerogel calcined at 923 K (a) aerogel, (b) xerogel

The comparative study of the aerogel and the xerogel by IR and RAMAN spectroscopies show that the calcination at higher temperatures causes the loss of sulphur for the two solids. This loss is increased for the xerogel. Hence, the sulphate species seem to be more stable at higher temperature for the aerogel.

The surface S/Zr ratio of the aerogel and xerogel obtained by the XPS spectroscopy are summarized in Table 3.

XPS surface analysis shows that the value of the S/Zr ratio of the aerogel heated at 833 K is more important than for the xerogel. At higher temperatures, there is an impoverishment in sulphur for the two solids, but this loss is greater for the xerogel. Thus the aerogel is able to retain more sulphur than the xerogel in the investigated temperature range. These results are keeping with those obtained by the other techniques.

4. Conclusion

The xerogel and aerogel samples were prepared by two methods of solvent evacuation. A comparative study of the textural and structural properties of these solids show that the method of solvent evacuation plays an important role in the stability of sulphur in the bulk and on the surface of the resulting materials. In fact, the aerogel, obtained by hypercritical drying develops the tetragonal phase just after solvent evacuation, whereas the xerogel is amorphous. The monoclinic phase appears after calcination at high temperature in the xerogel sample before the aerogel one. This result is related to the loss of sulphur, which is more important for the xerogel.

References

1. Hino M, Kobayashi S, Arata K (1979) J Am Chem Soc 101:6439
2. Li B, Gonzalez RD (1998) Appl Catal 174:109
3. Yaluris G, Larson RB, Kobe JM, Gonzalez R, Fogash KB, Dumesic JA (1996) J Catal 158:336
4. Ishida T, Yamagushi T, Tanabe K (1988) Chem Lett 1869
5. Tanabe K, Holderlich WK (1999) Appl Catal A 181:399
6. Yadav GD, Nair JJ (1999) Micropor Mesopor Mater 33:1
7. Hino M, Arata K (1980) J Chem Soc Chem Commun 851
8. Yamagushi T (1990) Appl Catal A 61:1
9. Davis BH, Keogh RA, Srinivasan R (1994) Catal Today 20:219
10. Guo C, Cao S, Qian Z (1994) Appl Cata A 107:229
11. Yadav GD, Thorat TS (1996) Ind Eng Chem Res 35:721
12. Clark JH, Monks GL, Nightingale DJ, Price PM, White JF (2000) J Catal 193:348
13. Quaschning V, Deutsch J, Druska P, Jiclas HJ, Kemnitz E (1998) J Catal 177:164
14. Yadav GD, Pujari AA (1999) Green Chem 1:69

15. Reddy BM, Sreekanth PM, Lakshmanan P (2005) J Mol Catal 237:93
16. Wakayama T, Matsuhashi H (2005) J Mol Catal 239:32
17. Watanabe K, Oshio N, Kawakami T, Kimura T (2004) App Catal 272:281
18. Spilbauer D, Mekhemer GH, Zaki MI, KnÖzinger H (1996) Catal Lett 40:41
19. Ward DA, Ko EI (1995) J Catal 157:321
20. Stichert W, Schüth F, Kuba S, KnÖzinger H (2001) J Catal 198:277
21. Arata K (1996) Appl Catal A 146:3
22. Ward DA, Ko EI (1995) J Catal 150:18
23. Tichit D, Coq B, Armendariz H, Figueras F (1996) Catal Lett 38:109
24. Younes MK, Ghorbel A, Rives A, Hubaut R (2000) J Sol Gel Sci Tech 19:81
25. Younes MK, Ghorbel A, Rives A, Hubaut R (2004) J Sol Gel Sci Tech 1:32
26. Hamouda LB, Ghorbel A (2000) J Sol Gel Sci Tech 19:413
27. Sing KSW, Everett DH, Haul RAW, Moscou L, Pierotti RA, Rouquerol J, Siemieniewska T (1985) P Appl Chem 57:603
28. Morterra C, Cerrato G, Signoretto M (1996) Catal Lett 36:129
29. Yamagushi T, Tanabe K, Kung YC (1986) Mater Chem Phys 16:67
30. Norman CJ, Goulding PA, McAlpine I (1994) Catal Today 20: 313
31. Vaudagna SR, Comelli RA, Figoli NS (1996) React Kinet Catal Lett 58:111
32. Parera JM (1992) Catal Today 15:481
33. Srinivasan R, Taulbee D, Davis BH (1991) Catal Lett 9:1
34. Stichert W, Schüth F (1998) Chem Mater 10:2020
35. Davids BH, Keagh RA, Srinivasan R (1994) Catal Today 20:219
36. Can L, Meijun L (2002) J Ram Specr 33:301
37. Keramidas VG, White WB (1974) J Am Ceram Soc 57:22
38. David AW, Ko EI (1993) Chem Mater 5:956
39. Signoretto M, Pinna F, Strukul G, Chies P (1997) J Catal 167:522
40. Babou F, Coudurier G, Vedrine J (1995) J Catal 152:341
41. Chackalackal S, Staffort FE (1966) J Am Chem Soc 88:723
42. Giguère G, Savoie R (1963) Cana J Chem 41:287
43. Bensitel M, Sauer O, Lavelly JC, Morrow BA (1988) Mater Chem Phys 19:147
44. Morterra C, Cerrato G, Signoretto M (1996) Catal Lett 41:101